ACS OMEGA

Open Access

http://pubs.acs.org/journal/acsodf

Article

Study on the Formation Mechanism of a Core−Shell Structure during Graphitization of Anthracite

Tian Qiu, Weining Xie, Xuejie Bai,* Chaoyong Li, and Ning Zhang

Cite This: *ACS Omega* 2024, 9, 22581−22589

Read Online

ACCESS | Metrics & More | Article Recommendations

ABSTRACT: Graphite is a revolutionary material, and the development of synthetic graphite could potentially solve the shortage of natural graphite in the future. In this paper, the formation of core−shell-structured synthetic graphite prepared from an anthracite−FeO mixture was systematically investigated by a two-step method. First, heat treatment was performed on a layer of almandine ($3FeO{\cdot}Al_2O_3{\cdot}3SiO_2$) particles to obtain a large quantity of uniform-sized glass-phase spheroids. Second, the deashed anthracite was graphitized on the surface of the obtained spheroids to prepare core−shell-structured graphite. Furthermore, the obtained graphite products were systematically characterized by XRD, Raman spectroscopy, SEM-EDS, and TEM. Finally, a model was proposed to illustrate the formation mechanism of the core−shell structure during graphitization of the anthracite−almandine mixture. Under lower temperatures, almandine started to melt into spheroids. Under higher temperatures, the volatile components in the anthracite turned into the gas phase, and the carbon matrix started to bend on the surface of the core material and deposit layer by layer, thus forming the core−shell-structured graphite. The findings could provide theoretical guidance for the synthetic graphite industry and have meaningful implications for the coal chemistry field.

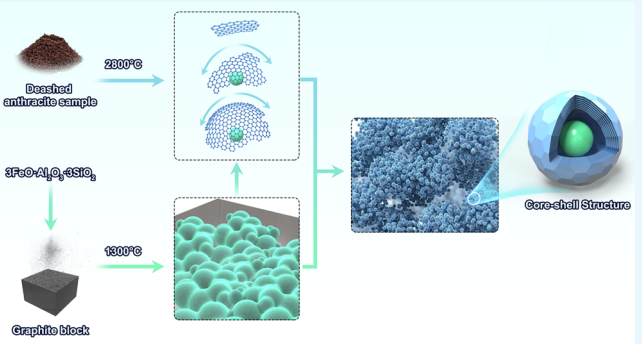

1. INTRODUCTION

The world has witnessed the emergence and development of graphite materials during the past few decades. As one of the revolutionary materials, graphite has many properties, such as high-temperature resistance, favorable thermal and electrical conductivity, outstanding lubricating characteristics, excellent chemical stability, etc., making it an irreplaceable material for many cutting-edge applications.[1] Graphite has been used in the aerospace industry because of its high-temperature resistance and strength performance. The favorable electrical conductivity and lower density make graphite ideal for the anode material of the lithium-ion battery and the electrical industry.[2,3] Graphite could perform an outstanding lubricating characteristic even under extremely high temperatures, which could outperform lubricating oil in the mechanical industry under certain circumstances.[4,5] More importantly, graphite with a porous structure could be used in energy storage composites, such as hydrogen storage materials and thermal storage materials.[6−8] Furthermore, graphite is an important precursor for the preparation of graphene, which is a new material with epoch-making significance.[9,10] However, the continuous increase in graphite consumption leads to a growing shortage of its natural resource, and the supply-demand mismatch will be a future challenge.[1] Hence, finding an efficient method to prepare synthetic graphite is in great demand and could potentially make up for the shortage of natural graphite resources in the long run.

In recent years, the study of synthetic graphite and its applications has become a hot topic in the research field.[11,12] A range of carbon sources with high carbon content and fewer impurities, e.g., petroleum coke,[13] coal tar pitch,[14] anthracite,[15] and bituminous coal,[12,16] were taken to prepare the synthetic graphite. Specifically, anthracite is one of the favorable resources for preparing synthetic graphite owing to its lower ash content and oxygen-containing functional groups.[15,17−19] Studies regarding coal-based synthetic graphite suggested that, with a lower rising rate of temperature and a higher final temperature, the obtained synthetic graphite tends to have a higher graphitization degree and perfect crystalline structure.[20,21] More importantly, the thermodynamics and kinetics of chemical reactions during the graphitization process of anthracite were investigated.[15] It is now well established from a

Received: December 1, 2023
Revised: February 25, 2024
Accepted: April 18, 2024
Published: May 16, 2024

https://doi.org/10.1021/acsomega.3c09596
ACS Omega 2024, 9, 22581−22589

Table 1. Proximate and Ultimate Analyses of Anthracite Samples[a]

anthracite samples	proximate analysis (wt %)			ultimate analysis (wt %, daf)				
	M_{ad}	A_d	V_{daf}	C	H	O	N	S
before deashing	1.07	4.23	7.86	87.04	3.11	8.59	0.62	0.64
after deashing	1.18	2.06	9.03	86.84	3.17	8.87	0.49	0.63

[a]M_{ad}: moisture (air-dry basis); A_d: ash (dry basis); V_{daf}: volatile (dry and ash-free basis); daf: dry and ash-free basis.

variety of studies that the operating parameters of a graphitization furnace could greatly affect the graphitization degree of the synthetic graphite product.[20−23] However, the effect of the mineral substance in the raw material on the graphitization process was often neglected, and the microstructural changes of the carbon matrix under high temperatures were less involved. A challenging problem that arises in this domain is that the correlation between the existing mineral content, especially common minerals such as quartz and pyrite, and the rearrangement of carbon atoms during graphitization has been inadequately established.

Notably, there are few studies on the graphitization mechanism of coal, but some researchers have made useful explorations of the graphitization process of a wider range of carbonaceous materials.[13,24−27] There is a growing awareness that, under high-temperature heat treatment, the evolution of carbonaceous materials into synthetic graphite is by no means a single process but a complicated procedure involving a variety of intermediate stages. Hence, many researchers have put forward a variety of conjectures, among which the most influential theories are carbide transformation theory,[28] recrystallization theory,[29] and microcrystal growth theory.[30]

In our previous work, it was found that the silica content in the raw material could facilitate the formation of the large flake graphite.[17] In addition, we also demonstrated that porous synthetic graphite with an onion-like structure could be successfully prepared from anthracite by adding Fe_2O_3 content, and its electrochemical performance as the anode material for lithium-ion batteries was systematically investigated.[31] However, the obtained graphite with a spherical structure was unevenly distributed in particle size, and the underlying mechanism of the microstructural change caused by the presence of Fe_xO_y has been insufficiently clarified. Hence, it is necessary to extend our research to a new level to reveal the regulation mechanism of Fe_xO_y during the graphitization of anthracite and repeatedly prepare spherical synthetic graphite with uniform particle size.

In this work, synthetic graphite with a core−shell structure was directionally prepared from anthracite by adding FeO to the raw material, and its underlying mechanism was adequately demonstrated by a two-step method. Specifically, almandine ($3FeO{\cdot}Al_2O_3{\cdot}3SiO_2$) particles were employed to prepare intermediate glass-phase spheroids. Then the spheroids were further used as the core material for the formation of the anthracite-based graphite with a core−shell structure. Furthermore, the microstructural changes of the obtained graphite were systematically characterized via a combination of X-ray diffraction (XRD), Raman spectroscopy, scanning electron microscopy (SEM), and transmission electron microscopy (TEM). Finally, the regulation mechanism of mineral components on the rearrangement of carbon atoms during the graphitization process was discussed in-depth. Based on the experimental findings, we proposed a model to illustrate the formation mechanism of the core−shell structure during the graphitization process of anthracite with the existence of almandine.

2. EXPERIMENTAL SECTION

2.1. Preparation of Spherical Anthracite-Based Graphite. The anthracite samples provided by the Taixi coal preparation plant (Ningxia, China) were employed as a carbon resource for the preparation of synthetic graphite. The proximate analysis and ultimate analysis of the Taixi anthracite can be found in Table 1. It could be seen that there is a range of associating minerals in the raw material that could potentially affect the graphitization process of the carbon matrix; thus, we remove the ash content in the anthracite samples as far as possible before the graphitization process. First, the anthracite samples were ground to obtain anthracite grains with a particle size of 74 μm. Subsequently, the anthracite grains were successively treated with alkali and acid to remove the impurities. The obtained anthracite grains were mixed with sodium hydroxide (Xilong Scientific, China) with a weight ratio of 2:1, which was further calcined in a muffle furnace at 150 °C for 10 h and subsequently rinsed with deionized water (DI) to remove excess sodium hydroxide. Then the obtained sample was dried at 120 °C for 12 h in a vacuum drying oven. Subsequently, the anthracite grains mixed with a 10% hydrochloric acid solution (Xilong Scientific, China) were placed in a water bath at 60 °C for 2 h. Finally, the deashed anthracite samples were obtained after rinsing with DI water until neutral. The proximate analysis and ultimate analysis of the deashed anthracite grains are listed in Table 1. After treatment with alkali and acid, the ash content in the anthracite decreased from 4.23 to 2.06%, showing that most of the impurities were removed during the deashing process.

It is noteworthy that the introduction of FeO was a supplement to Fe_2O_3 in our previous research,[31] aiming to decouple the microstructural change from the valence of the metal oxides. To investigate the effect of FeO on the microstructural changes in the carbon matrix during graphitization, FeO particles were added to the deashed anthracite grains to obtain anthracite−FeO mixtures with different mass ratios. Subsequently, the mixtures were placed in a graphite container inside a high-temperature graphitization furnace (Zhuzhou, China). During the graphitization process, high-purity argon was supplied to the furnace to purge the oxygen in the system, thus creating an atmosphere that was 20−30 kPa higher than the atmospheric pressure. The graphitization furnace was heated to 2800 °C at a rising rate of 10 °C/min. Subsequently, the temperature in the furnace was maintained for 3 h. The operating parameters for the graphitization of anthracite were based on our previous experimental research.[17] Finally, the anthracite-based graphite products could be obtained after the furnace was cooled to room temperature naturally. The obtained graphite products with different FeO contents (10, 20, 30, and 40%) were named

https://doi.org/10.1021/acsomega.3c09596
ACS Omega 2024, 9, 22581−22589

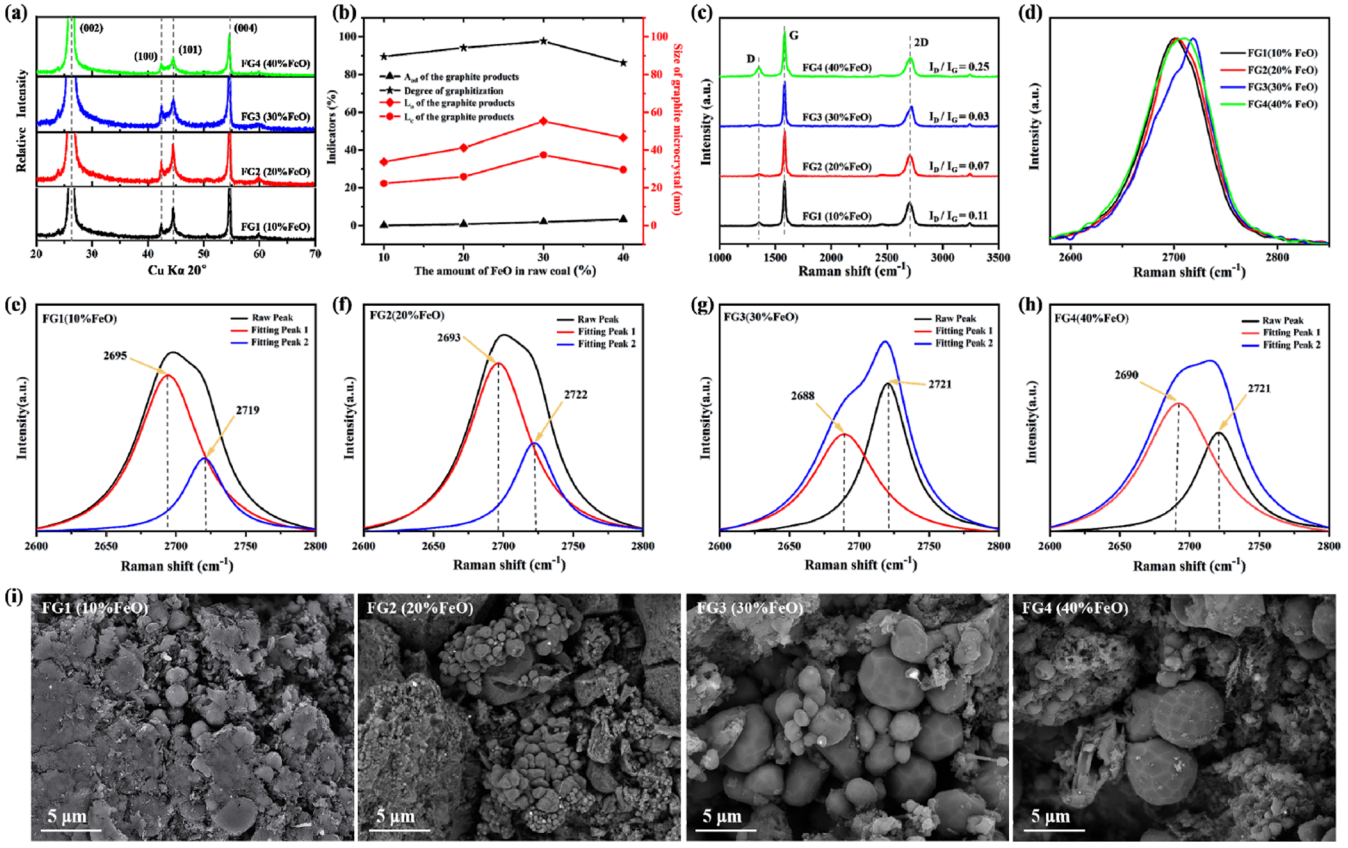

Figure 1. Effect of FeO content on the formation of spherical synthetic graphite prepared from deashed anthracite. (a) XRD spectra of the graphite products. (b) Graphitized lattice parameters and ash content of the graphite products as functions of FeO content in the mixture. (c) Raman spectra of the graphite products. (d) Second-order peaks of Raman spectra of the graphite products. (e–h) Peak-fitting second-order peaks of Raman spectra of the graphite products with FeO content ranging from 10 to 40%. (i) SEM images of the graphite products.

FG1, FG2, FG3, and FG4, respectively. These obtained graphite samples were further characterized by a combination of XRD, Raman spectroscopy, and SEM.

In addition, raw anthracite without the deashing process was employed to perform the graphitization process under high temperatures. The obtained anthracite-based graphite with a spherical structure was characterized by a combination of SEM-EDS, thus obtaining the correlation between the synthetic graphite's morphology and its *in situ* elemental distribution.

Finally, a two-step method was employed to further reveal the formation mechanism of the core–shell structure during the graphitization process of anthracite and associated minerals. During the first step, a layer of almandine ($3FeO{\cdot}Al_2O_3{\cdot}3SiO_2$), which is a product generated by commonly associated minerals at high temperatures, with a particle size of less than 74 μm was deposited on a small synthetic graphite block ($1 \times 1 \times 1$ cm^3). Then, the graphite–almandine sample was used for high-temperature treatment in a furnace, heating to 1300 °C. The obtained product was further characterized via SEM-EDS. During the second step, the obtained product was employed as the substrate material for the formation of uniform spherical graphite. A layer of deashed anthracite particles was deposited on the surface of the obtained product, which was further placed in the graphitization furnace, heating to 2800 °C, to obtain the synthetic graphite with an equal-sized core–shell structure. Furthermore, the obtained product was characterized by a combination of SEM, Raman spectrometry, XRD, and TEM.

2.2. Characterization of Anthracite-Based Graphite.

To characterize the microstructural changes of the obtained synthetic graphite, we systematically evaluated the anthracite-based graphite with a combination of XRD, Raman spectroscopy, SEM, and TEM. A Bruker D8 Advance diffractometer with the Cu Kα X-ray radiation source (λ = 0.15418 nm) was employed to obtain the X-ray diffraction spectra of the synthetic graphite products. During the measurement, the temperature was maintained at 55 ± 5 °C, and the X-ray intensities were measured as the diffraction varied between 10° and 80°. To calculate the interlayer spacing (d_{002}) of the graphite products from the (002) peak in the XRD pattern, Bragg's equation was introduced as follows:

$$d_{002} = \frac{\lambda}{2\sin\theta} \tag{1}$$

$$g = \frac{0.3440 - d_{002}}{0.3440 - 0.3354} \times 100\% \tag{2}$$

where d_{002} is the interlayer spacing, λ stands for the wavelength of the X-ray, θ denotes the Bragg angle that corresponds to the diffraction peak, g is the graphitization degree of the graphite product, 0.3354 and 0.3440 nm are the constants that represent the interlayer distance of the ideal single crystal graphite material and the original carbonaceous material, respectively.

Moreover, the Scherrer formula was introduced to calculate the stacking height and the crystallite size from the (002) and (110) peaks of the XRD patterns, respectively:

https://doi.org/10.1021/acsomega.3c09596
ACS Omega 2024, 9, 22581–22589

$$L_c = k_2\lambda/[\beta_{002}\cos\theta_{002}] \quad (3)$$

$$L_a = k_1\lambda/[\beta_{100}\cos\theta_{100}] \quad (4)$$

where L_c and L_a stand for stacking height and crystallite size, respectively, k_1 and k_2 are constants representing 1.84 and 0.94, respectively, and β is the full width at half-maximum (fwhm) of the diffraction peak.

Further, the degree of order of the obtained graphite product was evaluated by Raman spectroscopy. Here, a laser confocal Raman spectrometer (Bruker Senterra, Germany) was employed to obtain the Raman spectra of the synthetic graphite products. The Raman spectrometer was operating under a laser excitation of 632.8 nm (He−Ne laser, 1.96 eV), a power of 10 mW, and a laser wavelength of 514 nm, while the scanning range varied between 100 and 3500 cm^{-1}.

A field-emission SEM (Tescan, Czech Republic) coupled with an energy-dispersive spectrometer (EDS) was employed to observe the morphology of the obtained graphite materials. To increase the surface conductivity of the samples, a layer of gold was sputter-coated on the surface of the anthracite-based graphite before observation. Subsequently, the morphology and the *in situ* element distribution pattern could be simultaneously observed under the high vacuum mode of SEM-EDS.

A high-resolution TEM instrument (Tecnai G2 F20, FEI) was employed to investigate the microstructure and lattice parameters of the obtained graphite. Before TEM observation, the anthracite-based graphite was ground into powder and embedded in a resin, which was subsequently cut into nanosheets by an ultramicrotome and placed on a copper net for the TEM observation.

3. RESULTS AND DISCUSSION

Under a graphitization temperature of 2800 °C, synthetic graphite with a spherical structure could be obtained from the anthracite/FeO mixture, as clearly shown in Figure 1. Here, the effect of FeO on the rearrangement of carbon atoms during the graphitization process will be discussed in-depth via a combination of XRD, Raman, and SEM results.

Figure 1a shows the XRD spectra of the obtained synthetic graphite with different FeO contents. It is well-acknowledged that the (002) peak in the XRD spectra of graphite is determined by the spatial orientation of the aromatic ring carbon layer, while the (100) peak is attributed to the size of the aromatic ring carbon layer. Therefore, a sharper (002) peak indicates a better orientation of the aromatic ring carbon layer, and a sharper (100) peak leads to a larger size of the aromatic ring carbon layer.[16] As shown in Figure 1a, there was little difference between the (002) peaks in the XRD spectra of the obtained graphite, demonstrating that the graphitization process of the anthracite−FeO mixture could obtain highly ordered layer-structured graphite. However, the (100) peak in the XRD spectra of the obtained graphite changed significantly with varying FeO contents. Specifically, as the FeO content increased from 10 to 40%, the (100) peak first became sharp and strong, then turned to blunt and weak. To obtain a better understanding of the crystal structural change of anthracite during graphitization, the interlayer spacing (d_{002}), stacking height (L_c), crystallite size (L_a), and degree of graphitization (g) of the synthetic graphite with different FeO contents were systematically calculated, as can be seen in Table 2.

Table 2. Structural Parameters of the Anthracite-Based Graphite Products with Varying FeO Contents

samples	d_{002}, nm	L_a, nm	L_c, nm	g, %	A_{ad}, %
FG1	0.3363	33.7	22.3	89.2	0.12
FG2	0.3359	41.2	25.9	94.3	0.76
FG3	0.3357	55.3	37.4	96.9	1.98
FG4	0.3365	46.5	29.6	86.7	3.27

Meanwhile, industrial analysis was conducted on the obtained graphites. Here, ash content (A_d), graphitization degree (g), crystal plane size (L_a), and crystal packing height (L_c) of the obtained synthetic graphite as a function of FeO content in the raw material could be obtained, as shown in Figure 1b. With the continuous increase of FeO content, the graphitization degree (g), crystal plane size (L_a), and crystal packing height (L_c) of the synthetic graphite increased first and then decreased, while the ash content increased drastically. These results demonstrate that the appropriate addition of FeO could promote the growth of the carbon layers and that the arrangement of the aromatic ring carbon layer tends to be orderly structured. However, the excessive addition will hinder the growth of the graphite crystallinity, resulting in a decrease in the quality and purity of the graphite product. Combined with our previous findings,[31] it is demonstrated that the presence of FeO and Fe_2O_3 in the anthracite has a similar effect on the microstructure of the obtained graphite. Hence, the valence of the metal oxides has little influence on the microstructure of synthetic graphite obtained from anthracite.

Figure 1c shows the Raman spectra of synthetic graphite with varying FeO contents. For most carbon materials, there are two peaks in the first-order scattering of Raman spectroscopy: one at around 1580 cm^{-1} and the other at around 1350 cm^{-1}. The former is usually called peak G, representing the orderly structured and defect-free graphite, while the latter, often referred to as peak D, represents the graphite products with disordered structure and defects. The intensity ratio of the two peaks (I_D/I_G) reflects the degree of order for the crystalline structure of the carbon materials. As can be seen from Figure 1c, the G peaks of the obtained products for all cases were strong and sharp, indicating that the obtained graphite has a relatively complete layered-structure graphite crystalline. As the FeO content increased, the intensity of peak D for the corresponding graphite products reduced significantly, as shown in Figure 1c. This is mainly because the melting point of FeO was much lower than that of graphite and thus could escape from the system with the protective gas flow when the temperature reached up to 2800 °C. Hence, adding the appropriate amount of FeO could catalyze carbon recombination during the graphitization process. However, the excessive FeO content was unable to be discharged out of the reaction system, thus forming structure defects in graphite products due to the xenogeneic element occupation and enhancing the intensity of peak D in the Raman spectra.

It can be seen from Figure 1d that all of the synthetic graphite products have a second-order Raman peak located at around 2700 cm^{-1}. The smooth second-order Raman peak indicates that the synthetic graphite has formed a two-dimensional graphite lattice, while the three-dimensional lattice is imperfect. The unsmooth second-order Raman peak indicates that the three-dimensional graphite lattice has been developed, and the degree of perfection of the three-dimensional graphite lattice is proportional to the degree of

https://doi.org/10.1021/acsomega.3c09596
ACS Omega 2024, 9, 22581−22589

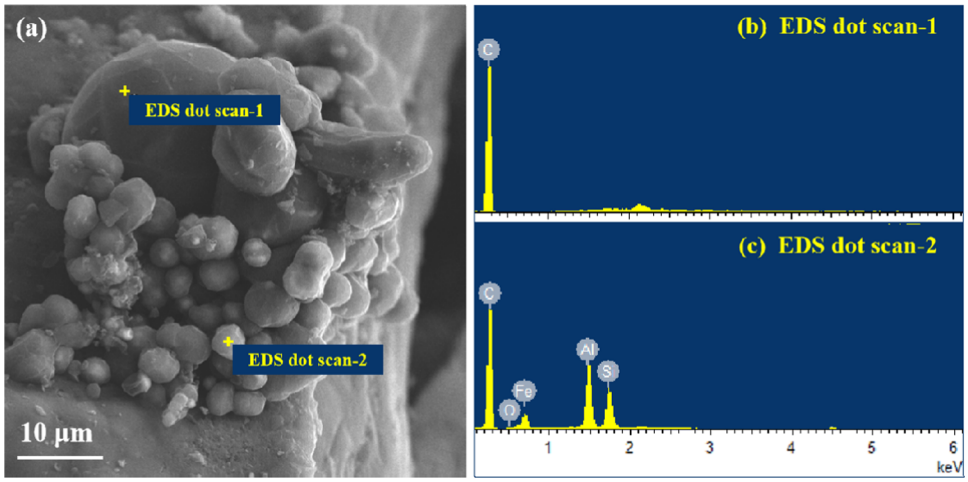

Figure 2. Morphology and *in situ* elemental distribution pattern of the obtained graphite prepared from raw anthracite. (a) SEM image of the obtained graphite. Elemental distribution pattern of (b) dot 1 and (c) dot 2 in the SEM image of the obtained graphite.

spectral peak splitting and the ratio of splitting peak intensity.[19] As can be seen from Figure 1e–h, with the increase of FeO content, both the degree of splitting of the second-order Raman peak and the intensity ratio of the splitting peak decreased gradually, which further demonstrates that FeO could remain in the product to form defects during the graphitization process.

To further study the microstructural change during the graphitization process, the morphology of the obtained graphite products was obtained via SEM, as illustrated in Figure 1i. It is shown that synthetic graphite with a sphere structure could be found in all cases, demonstrating that adding FeO to anthracite is beneficial for the formation of spherical graphite. More specifically, when the FeO content was 10%, only a small proportion of sphere-structured graphite could be found in synthetic graphite. As the FeO amount in the mixture increased gradually, more sphere-structured graphite was formed in the product and the size of spheroids grew accordingly, leading to uneven particle size for the spheroids. This is highly consistent with the XRD and Raman results. This further demonstrates that adding the appropriate amount of FeO was helpful in the formation of graphite spheroids with a uniform size. Therefore, preparing spherical graphite with a uniform size and revealing the formation mechanism of spherical graphite have become an important issue that needs to be addressed.

Since we repeatedly found that the Fe_xO_y in the raw material could facilitate the formation of spherical-structured graphite and this process was independent of the valence of Fe in Fe_xO_y, it is reasonable to assume that the introduction of iron ions could act as the core material for the growth of graphite during the graphitization process, where carbon atoms recombined on the surface of the core material layer by layer to form synthetic graphite with a core–shell structure. However, it seems that it is difficult to prepare synthetic graphite with uniform-sized spheres from iron ions alone; thus, we looked for other mineral elements that were conducive to the formation of spherical graphite from raw anthracite and verified the existence of the core–shell structure.

Here, a raw anthracite particle without the deashing process was used as the precursor to obtain the synthetic graphite. The morphology features and the elemental composition of the obtained synthetic graphite were observed via SEM-EDS, as can be seen in Figure 2. It is clearly shown that synthetic graphite particles with different sizes can be obtained. Subsequently, we perform the EDS measurement on the larger graphite and the smaller one separately, and the results can be found in Figure 2b,c, respectively. It is shown in Figure 2b,c that only carbon could be detected on the surface of the larger graphite particle, while C, Fe, Al, and Si could be found on the surface of the smaller one. It is interesting to note that the elemental composition of the obtained graphite particles is noticeably different. This disparity could have originated from the limitation of the detection depth of the EDS measurement, which could detect only several micrometers below the depth of the sample. The larger graphite particle is clearly beyond this limitation according to the scale bar of the SEM image, while the smaller one is in the detection range of the EDS measurement. Therefore, Fe-containing aluminosilicate in graphite, working as the core material for the smaller graphite, could be detected via EDS. However, the core material for the larger graphite was unable to be detected. This could demonstrate our assumption on the transformation of anthracite with the presence of Fe-containing aluminosilicate during graphitization: with increasing temperature, Fe-containing aluminosilicate started to melt into a spheroid, which could further work as the core material for the development of synthetic graphite. As the temperature continued to increase, the volatile components in the anthracite, mainly carbon and hydrogen, turned into the gas phase. Under higher temperatures, carbon and hydrogen elements started to deposit on the core material layer by layer, thus forming spherical synthetic graphite.

In our previous work, it was found that minerals in Taixi anthracite were mainly oxides, clay minerals, pyrite, carbonate, and sulfate, including quartz, kaolin, Illite, pyrite, calcite, and gypsum, among which pyrite is the main occurrence form of iron.[32] At high temperatures, pyrite will be oxidized to form wustite (FeO), hematite (Fe_2O_3), or magnetite (Fe_3O_4), and their melting point was in the range of 1530–1630 °C. Subsequently, it reacted with quartz and clay minerals to form glass-phase Fe-containing silica–aluminate. Compared with other valence states of iron, FeO could facilitate the formation of low-temperature eutectic of FeO, SiO_2, and Al_2O_3 to form iron olivine ($2FeO{\cdot}SiO_2$, melting point 1205 °C), iron spinel ($FeO{\cdot}Al_2O_3$, melting point 1780 °C), and almandine (3FeO·

https://doi.org/10.1021/acsomega.3c09596
ACS Omega 2024, 9, 22581–22589

$Al_2O_3{\cdot}3SiO_2$, melting point 1240−1300 °C). Since almandine is presented in the glass phase and its melting temperature range is much lower than that of ferrous oxide, it is more suitable for the core material of spherical graphite. The chemical reactions of pyrite, quartz, and clay minerals at high temperatures are described as follows:

$$2FeS_2 + 5O_2 \rightarrow 2FeO + 4SO_2 \quad (5)$$

$$4FeS_2 + 11O_2 \rightarrow 2Fe_2O_3 + 8SO_2 \quad (6)$$

$$3FeS_2 + 8O_2 \rightarrow Fe_3O_4 + 6SO_2 \quad (7)$$

$$FeO + SiO_2 \rightarrow FeO{\cdot}SiO_2 \quad (8)$$

$$FeO + FeO{\cdot}SiO_2 \rightarrow 2FeO{\cdot}SiO_2 \quad (9)$$

$$7FeO + 3Al_2O_3{\cdot}2SiO_2 \rightarrow 2(2FeO{\cdot}SiO_2) + 3(FeO{\cdot}Al_2O_3) \quad (10)$$

$$13FeO + 3(3Al_2O_3{\cdot}2SiO_2) \rightarrow 7(FeO{\cdot}Al_2O_3) + 2(3FeO{\cdot}Al_2O_3{\cdot}3SiO_2) \quad (11)$$

Given that almandine is a potentially suitable material for the core material of spherical graphite, we subsequently extended our research to validate that the presence of almandine is helpful to the formation of synthetic graphite with a uniform-sized core−shell structure. In this process, a two-step method was introduced: the core-forming step and the core−shell structure development step.

In the core-forming step, synthetic graphite with a layer of fine almandine particles was heated in the furnace, and the product was characterized via a combination of SEM-EDS. The morphology and *in situ* elemental distribution are given in Figure 3.

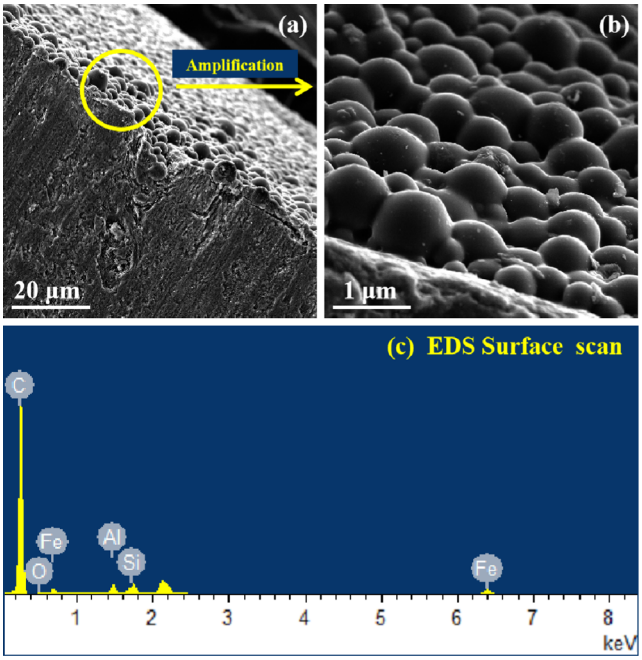

Figure 3. Morphology and *in situ* elemental distribution pattern of the obtained graphite prepared from synthetic graphite with a layer of almandine: (a) SEM image of the obtained graphite; (b) detailed SEM image of the selected area in panel (a); (c) elemental distribution pattern obtained from the SEM image in panel (b).

It could be seen from Figure 3a that after heat treatment at 1300 °C, large quantities of spherical graphite with a similar size range could be found on the surface of the synthetic graphite, where almandine particles were deposited. In contrast, areas without almandine coatings on another surface of the graphite remained intact. This is because almandine was melted in the furnace, thus forming a great number of uniform-sized spheroids.

The *in situ* EDS spectra show that elements Fe, Al, and Si could be found in the scanned range, demonstrating that the spheroids in the SEM image mainly originated from the almandine. It is also noteworthy that the element carbon in the spectra could be interference from the background. Both the heat treatment of the graphite−almandine mixture and the chemical reaction theory revealed that almandine could turn into a molten state during the temperature-rising process and the presence of molten almandine in the carbon source could potentially act as the core material for the growth of graphite during the graphitization process.

Given that the core material was successfully prepared by heating synthetic graphite with a layer of almandine, we further deposited a layer of anthracite particles on top of the obtained spheroids and performed the graphitization process, aiming to obtain uniform-sized graphite with a core−shell structure. Figure 4 gives the characterization of the synthetic graphite with a core−shell structure obtained from anthracite and almandine spheroids. It is worth noting that we compared the crystalline parameters of the obtained core−shell graphite (FSAG) with those of the synthetic graphite (FG3) obtained from the anthracite with 30% FeO content in Figure 1. Figure 4a shows the XRD spectra of FSAG and FG3. It can be seen that the intensity of the (100) peak in the FSAG spectrum was stronger than that of FG3, meaning that the obtained core−shell graphite had a larger-sized aromatic ring carbon layer, which symbolizes a more perfect graphite crystalline structure. Figure 4b shows the Raman spectra of FSAG and FG3. It is shown that the first-order peak D of the FSAG spectrum almost disappeared, demonstrating that the obtained core−shell graphite had fewer defects compared with FG3. As mentioned above, the unsmooth second-order peak in the Raman spectrum was better than that of the smooth peak, regarding the perfect degree of the three-dimensional graphite lattice. It is also clearly shown in Figure 4b that FG3 presented a smooth second-order peak, while FSAG had a split second-order peak. This also confirms that the obtained core−shell graphite developed a three-dimensional graphite lattice.

Figure 4c gives the morphology of the obtained graphite with a core−shell structure. It is shown that a large quantity of spherical graphite with a uniform size could be found in the obtained graphite, indicating that synthetic graphite with a spherical structure could be successfully prepared from anthracite and almandine via a two-step method. Furthermore, a TEM characterization was performed on the obtained graphite with a core−shell structure, as given in Figure 4d. It can be seen in the TEM image that there are abundant stripes with distinct boundaries in the selected area of the obtained graphite, meaning that the obtained graphite has a perfect layered structure. In addition, the diffraction pattern was circular, and the diffraction rings were clear and sharp, confirming that the obtained graphite had a perfect crystalline structure.

Here, based on our experimental results, we proposed a model to illustrate the formation mechanism of the core−shell

https://doi.org/10.1021/acsomega.3c09596
ACS Omega 2024, 9, 22581−22589

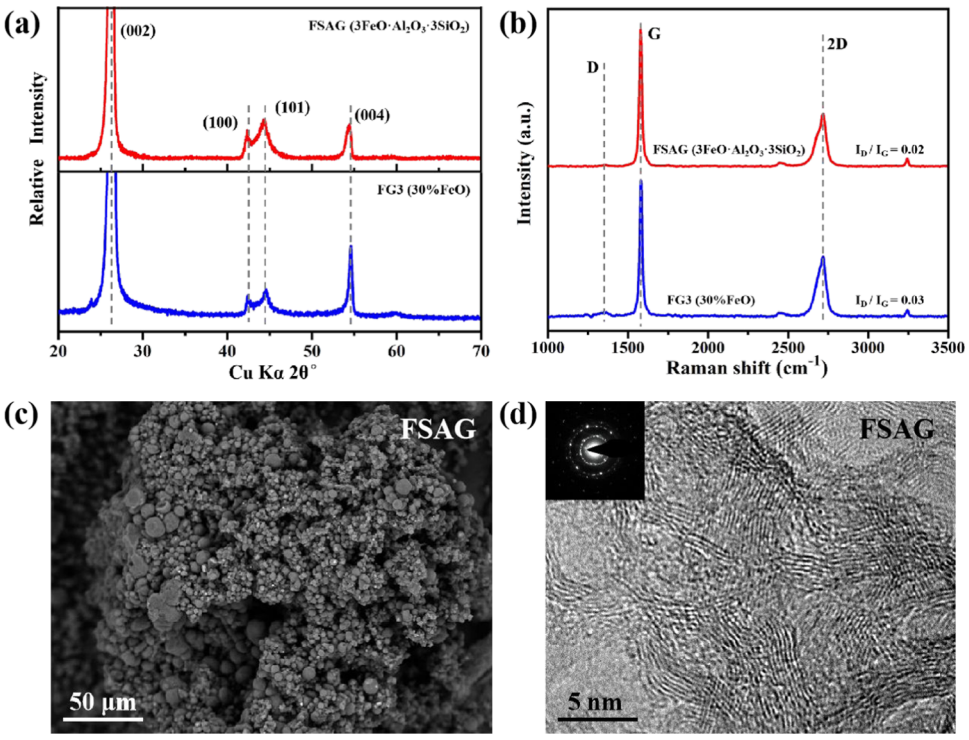

Figure 4. Characterization of the synthetic graphite with the core−shell structure obtained from anthracite and almandine spheroids. (a) XRD spectra of the graphite products; (b) Raman spectra of the graphite products; (c) SEM image of the graphite products; and (d) TEM image and corresponding diffraction patterns of the graphite products.

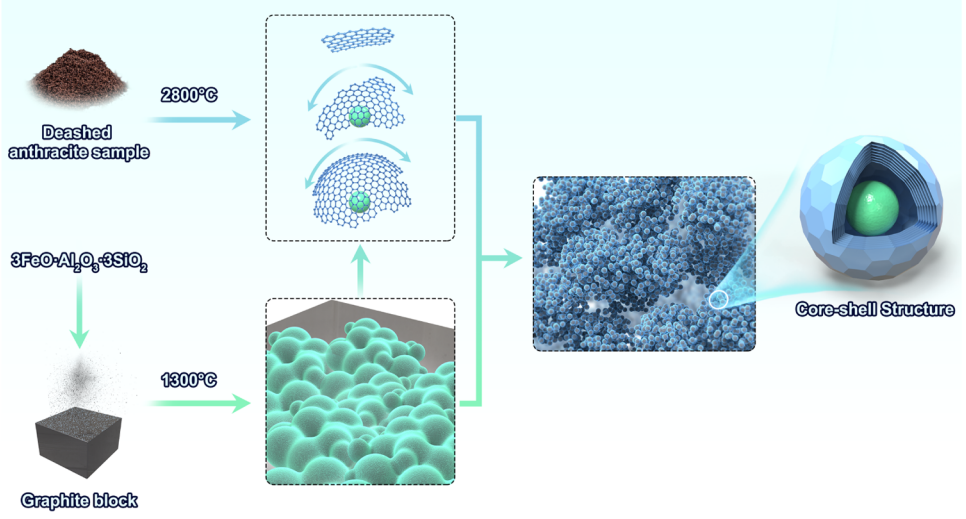

Figure 5. Model of the formation mechanism of the core−shell structure in synthetic graphite during the graphitization process of anthracite with the presence of associated minerals.

structure in the synthetic graphite during the graphitization process of anthracite with the presence of associated minerals. Under a temperature range of 1000−1300 °C, as shown in the left part of Figure 5, the iron-rich mineral $3FeO{\cdot}Al_2O_3{\cdot}3SiO_2$ in the anthracite turned into a molten state and became glass-phase spheroids. In our previous work, we found that the oxides of iron and silicon have catalytic effects on the graphitization process of anthracite. More specifically, graphite products with different structures, mainly polycrystalline graphite, monocrystalline graphite, spherical graphite, honeycomb graphite, and rod-like graphite, could be obtained by adjusting the associated minerals in the anthracite samples.[18] Furthermore, it was found that the presence of Fe_2O_3 content in anthracite could regulate the carbon matrix to form an onion-like structure.[19] Here, we further investigate the regulatory effects of these oxides on the microstructure of the graphitization process of anthracite. Thus, it is believed that the existence of spherical almandine, mainly consisting of Fe, Al, and Si, could act as the core material and facilitate the formation of a core−shell onion-like structure of graphite crystallized under high temperatures. With the presence of the graphite block, carbon and hydrogen atoms turned into the gas phase under 2800 °C and began to recombine on the spheroids, which is the core material of the onion-like

https://doi.org/10.1021/acsomega.3c09596
ACS Omega 2024, 9, 22581−22589

structure, to form graphite crystalline layer by layer, thus obtaining the core−shell synthetic graphite products, as shown in the middle part of Figure 5. With the presence of abundant almandine particles, a great deal of core−shell-structured graphite crystallinity, most of which are in the micrometer scale, could be obtained in the graphite products, as shown in the right part of Figure 5.

4. CONCLUSIONS

In conclusion, synthetic graphite with a core−shell structure was successfully prepared from anthracite, and a regulating mechanism of the associated minerals in the raw material during graphitization was proposed. First, synthetic graphite with a spherical structure was obtained from anthracite by adjusting the FeO content in the mixture. Then, raw anthracite particles without the deashing process were used as the precursor to prepare synthetic graphite with a spherical structure. In addition, a two-step method was introduced to prepare the graphite with a core−shell structure, namely, the formation of the intermediate spheroids (step 1) and the development of the synthetic graphite with a core−shell structure (step 2). Furthermore, a combination of XRD, Raman spectroscopy, SEM-EDS, and TEM was employed to characterize the obtained graphite.

The results suggest that adding the appropriate amount of FeO to the anthracite could promote the growth of the carbon layers during graphitization and form orderly structured graphite products. However, the excessive addition of FeO results in a decrease in the quality and purity of graphite products. In addition, the valence of the metal oxides was decoupled from microstructural changes in synthetic graphite. Further, it was demonstrated that synthetic graphite particles with various particle sizes could be obtained from the graphitization process of raw anthracite particles without deashing. Based on SEM-EDS characterization of a larger graphite particle and a smaller one, we proposed an assumption that a core−shell structure could be formed during the graphitization process. To validate this assumption, we first deposited almandine particles on synthetic graphite and performed heat treatment under 1300 °C to form intermediate glass-phase spheroids. Second, the spheroids with a layer of anthracite particles were placed in the graphitization furnace and heated up to 2800 °C, thus successfully obtaining uniform-sized synthetic graphite with a core−shell structure.

Finally, a model was proposed to demonstrate the formation mechanism of the synthetic graphite with a core−shell structure during the graphitization process of anthracite, with the existence of associated minerals. Within a lower temperature range, associated minerals in the anthracite turned to a molten state and became glass-phase spheroids. These spheroids further act as the core material for the growth of graphite crystalline. Under higher temperatures, carbon and hydrogen atoms in the anthracite turned to the gas phase. Under graphitization temperatures, volatile components, including carbon and hydrogen atoms in the system, began to recombine on the core material to form graphite crystalline layer by layer, thus obtaining the synthetic graphite with a core−shell structure.

AUTHOR INFORMATION

Corresponding Author

Xuejie Bai − *School of Mechanical & Electrical Engineering, Xuzhou University of Technology, Xuzhou 221018 Jiangsu, China*; orcid.org/0009-0003-4365-9163; Email: baixuejie@xzit.edu.cn

Authors

Tian Qiu − *School of Mechanical & Electrical Engineering, Xuzhou University of Technology, Xuzhou 221018 Jiangsu, China*

Weining Xie − *Advanced Analysis & Computation Center, China University of Mining and Technology, Xuzhou 221116 Jiangsu, China; School of Chemical Engineering and Technology, China University of Mining and Technology, Xuzhou 221116 Jiangsu, China*; orcid.org/0000-0002-6048-5121

Chaoyong Li − *School of Mechanical & Electrical Engineering, Xuzhou University of Technology, Xuzhou 221018 Jiangsu, China*

Ning Zhang − *School of Mechanical & Electrical Engineering, Xuzhou University of Technology, Xuzhou 221018 Jiangsu, China*

Complete contact information is available at: https://pubs.acs.org/10.1021/acsomega.3c09596

Notes

The authors declare no competing financial interest.

ACKNOWLEDGMENTS

This work was supported by the Natural Science Foundation of Jiangsu Province (BK20210506). The authors would like to thank the Advanced Analysis and Computation Center of the China University of Mining and Technology for their technical support.

REFERENCES

(1) Jara, A. D.; Betemariam, A.; Woldetinsae, G.; Kim, J. Y. Purification, Application and Current Market Trend of Natural Graphite: A Review. *Int. J. Min. Sci. Technol.* **2019**, *29* (5), 671−689.

(2) Zhao, L.; Ding, B. C.; Qin, X. Y.; Wang, Z. J.; Lv, W.; He, Y. B.; Yang, Q. H.; Kang, F. Y. Revisiting the Roles of Natural Graphite in Ongoing Lithium-Ion Batteries. *Adv. Mater.* **2022**, *34* (18), No. 2106704.

(3) Yang, J. B.; Fan, E. S.; Lin, J.; Arshad, F.; Zhang, X. D.; Wang, H. Y.; Wu, F.; Chen, R. J.; Li, L. Recovery and Reuse of Anode Graphite from Spent Lithium-Ion Batteries via Citric Acid Leaching. *ACS Appl. Energy Mater.* **2021**, *4* (6), 6261−6268.

(4) Omrani, E.; Moghadam, A. D.; Menezes, P. L.; Rohatgi, P. K. Influences of Graphite Reinforcement on the Tribological Properties of Self-lubricating Aluminum Matrix Composites for Green Tribology, Sustainability, and Energy Efficiency-A Review. *Int. J. Adv. Manuf. Technol.* **2016**, *83* (1−4), 325−346.

(5) Li, B.; Jiang, X. F.; Wu, Y. P.; Wan, H. Q.; Chen, L.; Ye, Y. P.; Zhou, H. D.; Chen, J. M. Novel Environmental-friendly Lubricating Materials: Water-based PAI-graphite-LaF3 Bonded Solid Lubricating Coatings. *Appl. Surf. Sci.* **2019**, *481*, 900−909.

(6) Singh, D.; Yu, W. H.; Zhao, W. H.; Kim, T.; France, D. M.; Smith, R. K. Development and Prototype Testing of MgCl2/graphite Foam Latent Heat Thermal Energy Storage System. *Sol. Energy* **2018**, *159*, 270−282.

(7) Niyomsoan, S.; Leiva, D. R.; Silva, R. A.; Chanchetti, L. F.; Shahid, R. N.; Scudino, S.; Gargarella, P.; Botta, W. J. Effects of Graphite Addition and Air Exposure on Ball-milled Mg-Al Alloys for Hydrogen Storage. *Int. J. Hydrogen Energy* **2019**, *44* (41), 23257−23266.

(8) Barthwal, M.; Dhar, A.; Powar, S. Effect of Nanomaterial Inclusion in Phase Change Materials for Improving the Thermal Performance of Heat Storage: A Review. *ACS Appl. Energy Mater.* **2021**, *4* (8), 7462−7480.

(9) Zhang, Y.; Peng, W. J.; Xia, L.; Song, S. X. Adsorption of Cd(II) at the Interface of Water and Graphene Oxide Prepared from Flaky Graphite and Amorphous Graphite. *J. Environ. Chem. Eng.* **2017**, *5* (4), 4157−4164.
(10) Zhang, W. X.; Liu, Z. P.; Xia, J.; Li, F.; He, W. Z.; Li, G. M.; Huang, J. W. Preparing Graphene from Anode Graphite of Spent Lithium-ion Batteries. *Front. Environ. Sci. Eng.* **2017**, *11* (5), 6.
(11) Cao, D. Y.; Wang, L.; Ding, Z. Y.; Peng, Y. W.; Li, Y. Characterization of the Heterogeneous Evolution of the Nanostructure of Coal-Based Graphite. *J. Nanosci. Nanotechnol.* **2021**, *21* (1), 670−681.
(12) Wang, L. P.; Yao, Z. X.; Guo, Z. M.; Shen, X. F.; Li, Z. A.; Zhou, Z. Q.; Wang, Y. L.; Yang, J. G. Effects of Solvent Extraction on the Microstructure of Bituminous Coal-based Graphite. *Carbon Lett.* **2022**, *32* (3), 741−749.
(13) Nugroho, A.; Nursanto, E. B.; Pradanawati, S. A.; Oktaviano, H. S.; Nilasary, H.; Nursukatmo, H. Fe Based Catalysts for Petroleum Coke Graphitization for Lithium Ion Battery Application. *Mater. Lett.* **2021**, *303*, No. 130557.
(14) Wang, Q. L.; He, M.; Li, X. C.; Hao, L. Preparation and Properties of Graphite/Antimony Composites Based on Coal Tar Pitch. *Adv. Compos. Lett.* **2017**, *26* (2), 49−55.
(15) Qiu, T.; Yang, J.-g.; Bai, X.-j. Insight into the Change in Carbon Structure and Thermodynamics during Anthracite Transformation into Graphite. *Int. J. Min. Met. Mater.* **2020**, *27* (2), 162−172.
(16) Xing, B.; Zhang, C.; Cao, Y.; Huang, G.; Liu, Q.; Zhang, C.; Chen, Z.; Yi, G.; Chen, L.; Yu, J. Preparation of synthetic graphite from bituminous coal as anode materials for high performance lithium-ion batteries. *Fuel Process. Technol.* **2018**, *172*, 162−171.
(17) Qiu, T.; Yang, J.-G.; Bai, X.-J. Investigation on microstructural changes of Anthracite during Graphitization and effect of Silica content on product crystal structure. *Energy Sources, Part A* **2021**, *43* (7), 769−782.
(18) Qiu, T.; Yang, J.-G.; Bai, X.-J. Preparation of Coal-based Graphite with Different Microstructures by Adjusting the Content of Ash and Volatile Matter in Raw Coal. *Energy Sources, Part A* **2020**, *42* (15), 1874−1881.
(19) Qiu, T.; Yang, J.-G.; Bai, X.-J.; Wang, Y.-L. The Preparation of Synthetic Graphite Materials with Hierarchical Pores from Lignite by One-step Impregnation and their Characterization as Dye Absorbents. *RSC Adv.* **2019**, *9* (22), 12737−12746.
(20) González, D.; Montes-Morán, M.; Young, R. J.; Garcia, A. Effect of Temperature on the Graphitization Process of a Semi-anthracite. *Fuel Process. Technol.* **2002**, *79* (3), 245−250.
(21) Weisenberger, M.; Martin-Gullon, I.; Vera-Agullo, J.; Varela-Rizo, H.; Merino, C.; Andrews, R.; Qian, D.; Rantell, T. The Effect of Graphitization Temperature on the Structure of Helical-ribbon Carbon Nanofibers. *Carbon* **2009**, *47* (9), 2211−2218.
(22) González, D.; Montes-Morán, M. A.; Suárez-Ruiz, I.; Garcia, A. B. Structural Characterization of Graphite Materials Prepared from Anthracites of Different Characteristics: A Comparative Analysis. *Energy Fuels* **2004**, *18* (2), 365−370.
(23) Shyam Kumar, C. N.; Chakravadhanula, V. S. K.; Riaz, A.; Dehm, S.; Wang, D.; Mu, X.; Flavel, B.; Krupke, R.; Kübel, C. Understanding the Graphitization and Growth of Free-standing Nanocrystalline Graphene using in situ Transmission Electron Microscopy. *Nanoscale* **2017**, *9* (35), 12835−12842.
(24) Boubiche, N.; El Hamouchi, J.; Hulik, J.; Abdesslam, M.; Speisser, C.; Djeffal, F.; Le Normand, F. Kinetics of Graphitization of Thin Diamond-like Carbon (DLC) Films Catalyzed by Transition Metal. *Diamond Relat. Mater.* **2019**, *91*, 190−198.
(25) Xia, S. W.; Cai, N.; Lu, W.; Zhou, H. W.; Xiao, H. Y.; Chen, X.; Chen, Y. Q.; Yang, H. P.; Wang, X. H.; Wang, S. R.; Chen, H. P. Reaction Kinetics, Mechanism, and Product Analysis of the Iron Catalytic Graphitization of Cellulose. *J. Cleaner Prod.* **2021**, *329*, No. 129735.
(26) Li, K. J.; Zhang, J. L.; Liu, Y. X.; Barati, M.; Liu, Z. J.; Zhong, J. B.; Su, B. X.; Wei, M. F.; Wang, G. W.; Yang, T. J. Graphitization of Coke and Its Interaction with Slag in the Hearth of a Blast Furnace. *Metall. Mater. Trans. B* **2016**, *47* (2), 811−818.
(27) Nakamura, Y.; Yoshino, T.; Satish-Kumar, M. Pressure Dependence of Graphitization: Implications for Rapid Recrystallization of Carbonaceous Material in a Subduction Zone. *Contrib. Mineral. Pet.* **2020**, *175* (4), 32.
(28) Pappano, P. J.; Schobert, H. H. Effect of Natural Mineral Inclusions on the Graphitizability of a Pennsylvania Anthracite. *Energy Fuels* **2009**, *23* (1), 422−428.
(29) Oberlin, A.; Terriere, G. Graphitization Studies of Anthracites by High Resolution Electron Microscopy. *Carbon* **1975**, *13* (5), 367−376.
(30) Franklin, R. E. Crystallite Growth in Graphitizing and Non-Graphitizing Carbons. *Proc. R. Soc. A* **1951**, *209* (1097), 196−218, DOI: 10.1098/rspa.1951.0197.
(31) Qiu, T.; Yu, Z. Y.; Xie, W. N.; He, Y. Q.; Wang, H. F.; Zhang, T. Preparation of Onion-like Synthetic Graphite with a Hierarchical Pore Structure from Anthracite and Its Electrochemical Properties as the Anode Material of Lithium-Ion Batteries. *Energy Fuels* **2022**, *36* (15), 8256−8266.
(32) Wang, L. P.; Qiu, T.; Guo, Z. M.; Shen, X. F.; Yang, J. G.; Wang, Y. L. Changes and Migration of Coal-Derived Minerals on the Graphitization Process of Anthracite. *ACS Omega* **2021**, *6* (1), 180−187.

https://doi.org/10.1021/acsomega.3c09596
ACS Omega 2024, 9, 22581−22589